

# Holographic image reconstruction by a Josephson junction

Razmik A. Hovhannisyan, Taras Golod, and Vladimir M. Krasnov\*

*Department of Physics, Stockholm University, AlbaNova University Center, SE-10691 Stockholm, Sweden*

A general problem of magnetic sensors is a trade-off between spatial resolution and field sensitivity: with decreasing sensor size the resolution is improved but the sensitivity is deteriorated. Here we present a novel method of magnetic image reconstruction by a single Josephson junction, which can resolve the problem. The method resembles holography, with the diffraction-like  $I_c(H)$  pattern serving as a hologram. It represents an example of quantum holography of electronic wave functions, corresponding in this case to the macroscopic superconducting condensate. We show theoretically and verify experimentally that the method allows super-resolution imaging with a nm-scale spatial resolution not limited by the junction size. We demonstrate that planar Josephson junctions facilitate both high field sensitivity and high spatial resolution, thus obviating the trade-off problem in magnetic scanning probe imaging.

Magnetic scanning probe microscopy (SPM) has been rapidly developing in recent decades. Magnetic force (MFM) [1–7], Superconducting Quantum Interference Device (SQUID) [8–16], Hall-probe [17, 18] and NV-center [19–23] microscopies achieved remarkable advances. However, many magnetic sensors suffer from the trade-off problem between spatial resolution and magnetic field sensitivity. For example, SQUIDs detect a fraction of the flux quantum,  $\Phi_0$  [8, 24]. Therefore, their field sensitivity is inversely proportional to the pickup loop area, while spatial resolution is determined by the loop size. Thus, miniaturization leads to improvement of resolution at the expense of sensitivity.

Coherent nature of the superconductivity enables observation of quantum-mechanical phenomena in macroscopic objects [25, 26]. Josephson effect appears as a result of electronic wave function interference between two superconducting electrodes [27]. It leads to diffraction-like Fraunhofer modulation of the critical current as a function of magnetic field,  $I_c(H)$ . In Ref. [28] it was proposed to use a single sandwich-type Josephson junction (JJ) as an SPM sensor. This enables ultimate miniaturization and improves spatial resolution [13], but the trade-off problem persists. In Ref. [29] it was argued that planar JJs [30, 31] would allow at least partial obviation of the problem. Local magnetic field,  $H^*(x)$ , leads to distortion of  $I_c(H)$  [32] and  $H^*(x)$  is encoded in the shape of  $I_c(H)$ . Restoration of this information would allow super-resolution imaging not limited by the JJ size [32]. This requires solution of an inverse problem - reconstruction of unknown  $H^*(x)$  from the known  $I_c(H)$ .

In this work we show both theoretically and experimentally that magnetic field distribution in a JJ can be reconstructed via inverse Fourier transform of the  $I_c(H)$  pattern. The method resembles the Fourier-transform holography [33–35], with diffraction-like  $I_c(H)$  patterns serving as holograms. It represents an example of quantum holography [36], involving in our case electronic wave functions of superconducting condensates. We demon-

strate that the method enables super-resolution imaging independent of the junction size and limited only by the  $I_c(H)$  field range. Experimental verification is performed using Nb-CuNi-Nb planar JJs. We analyze the field profile from the MFM tip and confirm the accuracy of reconstruction  $\sim 20$  nm using a calibrated case of stray fields from an Abrikosov vortex (AV) [37, 38]. We conclude that the holographic imaging by planar JJs facilitates both high field sensitivity and high spatial resolution, thus obviating the trade-off problem in SPM.

Figure 1 shows a sketch of SPM experiment: a small object with local field  $H^*$  is imaged by a JJ. We assume that the JJ is “short” and does not screen the field. The direct problem, i.e., calculation of  $I_c(H)$  for a given  $H^*(x)$ , was solved in Ref. [32]. The field induces a gradient of Josephson phase shift,  $d\varphi/dx = \alpha H_y$ . A small magnetic object creates a step-like phase shift,

$$\varphi^*(x) = \alpha \int_0^x H^*(\xi) d\xi. \quad (1)$$

$I_c$  is obtained by maximization of the Josephson current,

$$I_c = \int_{-L/2}^{L/2} J_c(x) \sin[\alpha H x + \varphi^*(x) + \varphi_0] dx, \quad (2)$$

with respect to  $\varphi_0$ . Here  $J_c(x)$  is the critical current density, which may vary along the JJ [39, 40]. Our goal is to solve the inverse problem: reconstruct  $H^*(x)$  from a given  $I_c(H)$ . Below we briefly describe our approach with more details available in the Supplementary [41].

Application of the inverse Fourier transform to Eq. (2) yields a system of two equations for  $\varphi^*(x)$  [41]:

$$J_c(x) \sin[\varphi^*(x)] = \frac{\alpha}{2\pi} \int_{-\infty}^{\infty} \cos[\alpha x H + \varphi_0(H)] I_c(H) dH, \quad (3)$$

$$J_c(x) \cos[\varphi^*(x)] = \frac{\alpha}{2\pi} \int_{-\infty}^{\infty} \sin[\alpha x H + \varphi_0(H)] I_c(H) dH. \quad (4)$$

\* vladimir.krasnov@fysik.su.se

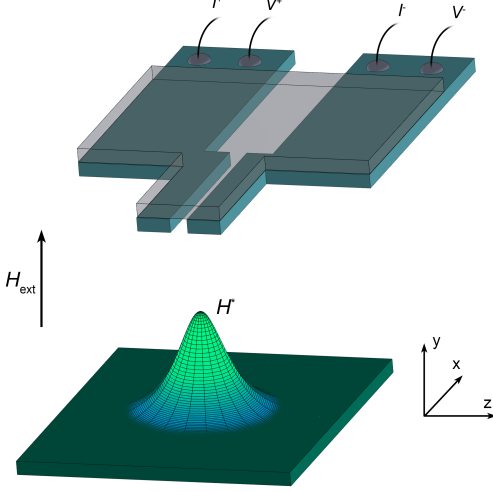


FIG. 1. A sketch of the considered SPM experiment. A planar Josephson junction is employed as a sensor for imaging of a small magnetic objects with a local field  $H^*$ .

The unknown  $\varphi_0(H)$  should be obtained from the maximization criterion,  $\partial I_c / \partial \varphi_0 = 0$ , which gives:

$$\varphi_0(H) = \frac{\pi}{2} - \arctan \left[ \frac{A(H)}{B(H)} \right]. \quad (5)$$

Here  $A(H) = \int_{-L/2}^{L/2} J_c(x) \sin[\alpha H x + \varphi^*(x)] dx$  and  $B(H) = \int_{-L/2}^{L/2} J_c(x) \cos[\alpha H x + \varphi^*(x)] dx$ . In the absence of the object,  $\varphi^* = 0$ , for a uniform JJ,  $J_c(x) = I_{c0}/L$ , the term  $A$  vanishes because the integrand is odd in  $x$ . In this case, Eq. (5) yields  $\varphi_0 = \pi/2$  and  $I_c(f)$  exhibits Fraunhofer modulation,  $I_{c0} \sin(\pi f)/\pi f$ , where  $f = \Phi/\Phi_0 = H/H_0$  is the normalized flux and  $H_0$  is the flux quantization field. Substitution of  $\varphi_0 = \pi/2$  and the Fraunhofer  $I_c(H)$  in Eqs. (3,4) leads to  $\sin(\varphi^*) = 0$ ,  $\cos(\varphi^*) = 1$ , verifying reconstruction of the trivial case.

For  $H^* \neq 0$ ,  $\varphi_0$  may depend both on  $H$  and  $H^*$  [41], preventing a straightforward solution. As usual, the inverse problem requires additional knowledge about the object. In SPM we are primarily interested in imaging of small magnetic objects, such as vortices or domain walls, with spatially symmetric  $H^*(x)$ . When a symmetric object is placed in the middle of a JJ with a symmetric  $J_c(x)$ , the term  $A(H)$  in Eq. (5) vanishes again, so that  $\varphi_0 = \pi/2$  and the inverse solution, Eqs. (3,4), remains unambiguous. The most accurate reconstruction is achieved using  $\tan[\varphi^*]$  obtained by solving both Eqs. (3) and (4). Mutual division of Eqs. (3) and (4) eliminates the  $J_c(x)$  term. This is important for practical application when  $J_c(x)$  is not confidently known. All solutions presented below are obtained this way.

To verify the method, first we consider the well calibrated case of AV. Vortex stray fields induce the Josephson phase shift [37, 42],

$$\varphi^*(x) = -V \arctan \left( \frac{x - x_v}{|z_v|} \right). \quad (6)$$

Here  $V$  is the vorticity, and  $x_v, z_v$  are AV coordinates. Figure 2 (a) shows the calculated total flux induced by AV at different locations  $(x_v, z_v)$  [29]. It corresponds to SPM scan with zero height,  $y_v = 0$ . When the JJ approaches the vortex along the middle line,  $x = 0$ , the growing induced flux and phase shift  $\varphi^*$ , Eq. (6), lead to a progressive shift and distortion of  $I_c(H)$  patterns [32, 37, 38, 42]. This is shown in Fig. 2 (b) for three positions of an antivortex, indicated by arrows. Dashed black lines in Fig. 2 (c) represent inverse problem solutions,  $H^*(x)$ , reconstructed from these  $I_c(H)$  patterns. They coincide with the actual profiles, shown by blue, olive and red lines in Fig. 2 (c), confirming the successful image reconstruction. Interestingly, unlike a conventional pixel-by-pixel SPM scanning, here the complete one-dimensional distribution  $H^*(x)$  within the JJ is obtained at once. Therefore, it would be sufficient to scan just in  $z$ -direction to obtain the full two-dimensional  $H^*(x, z)$  map, speeding up the imaging process.

For experimental verification we use planar Nb-CuNi-Nb JJs, as shown in Figure 3 (d). Several devices were studies, each containing one or two JJs with the lengths  $L \simeq 5.4 \mu\text{m}$  and a vortex trap in the middle of the electrode,  $x_v = 0$ , at different distances,  $z_v$ , from the JJs. Details about device fabrication, characterization and the experimental setup can be found in Refs. [29, 31, 37, 42] and the Supplementary [41]. Black symbols in Fig. 3 (a-c) show measured  $I_c(H)$  patterns at  $T \simeq 6.6 \text{ K}$ , (a) in the absence of a vortex, and with a trapped antivortex at (b)  $z_v = 0.94 \mu\text{m}$  and (c)  $z_v = 0.36 \mu\text{m}$ . A progressive distortion, similar to that in Fig. 2 (b) can be seen. Red lines represents fits using  $\varphi^*$  from Eq. (6) with the actual  $L, x_v$  and  $z_v$  and the prefactor  $V$  as the only fitting parameter [37]. Black line in Fig. 3 (e) represents the reconstructed AV field, obtained from the experimental  $I_c(H)$  from (c). The red line shows the expected  $H^*(x)$  obtained from the fit using Eq. (6) in Fig. 3 (c). The quantitative agreement is apparent. The width at half-maximum of the reconstructed  $H^*(x)$  is  $\sigma \sim 500 \text{ nm} \lesssim 0.1 L$ , confirming the super-resolution ability of the method. However, the accuracy of reconstruction is much better than  $\sigma$ . The inset in Fig. 3 (e) shows a close-up on the half-maximum region. It is seen that the discrepancy of fitted and reconstructed profiles is  $\Delta\sigma \simeq 20 \text{ nm}$ . It represents the actual spatial resolution of the method.

As shown in the Supplementary [41], the resolution is limited only by the maximum flux range  $\Phi/\Phi_0$ , i.e., the number of lobes in  $I_c(H)$ . In Fig. 3 (f) we show the relative accuracy of reconstruction of the width,  $\Delta\sigma/\sigma$ , and the height,  $\Delta H^*/H^*(0)$ , as a function of the inverse flux range. It can be seen that the accuracy of both quantities rapidly improves for  $\Phi/\Phi_0 > 5$  and practically vanishes

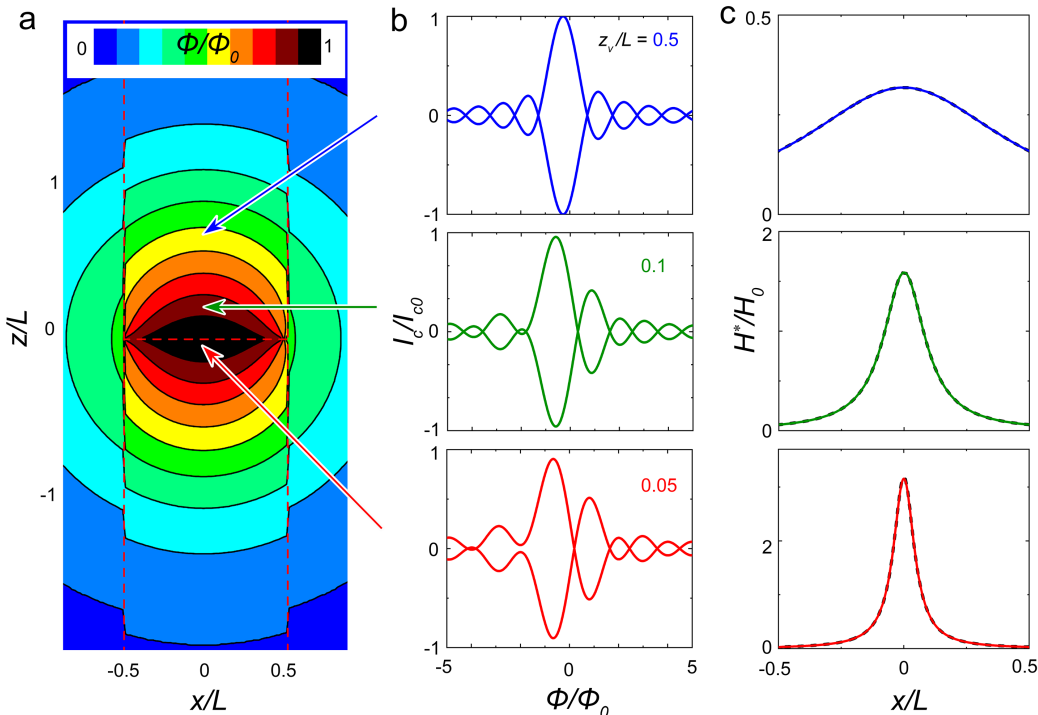


FIG. 2. Numerical modeling of SPM of an Abrikosov antivortex. (a) The total flux induced by AV in a junction, as a function of its position  $(x_v, z_v)$ . Vertical dashed lines mark edges of electrodes, the horizontal dashed line in the middle represents the junction. Data from Ref. [29]. (b) Calculated  $I_c(H)$  patterns for three locations of the AV with respect to the junction, indicated by arrows. (c) Profiles of stray fields induced by AV. Black dashed lines show reconstructed  $H^*(x)$  from  $I_c(H)$  patterns in (b). They coincide with solid (blue, olive and red) lines, representing actual fields obtained from Eq. (6).

for  $\Phi/\Phi_0 > 10$ . The experimental reconstruction in Fig. 3 (e) is made for  $\Phi/\Phi_0 = \pm 8$ , see Fig. 3 (c), which is enough to achieve the remarkable  $\sim 20$  nm accuracy.

Our method resembles the Fourier-transform holography [33–35], with diffraction-like  $I_c(H)$  patterns serving as holograms. In holography the image quality increases with increasing the size of the hologram, i.e., with increasing the number of stored interference fringes. In our case the number of fringes corresponds to the number of lobes, i.e., to the flux range  $\Phi/\Phi_0$ . However, the specifics of our case is that the hologram is created by interference of the object with electronic wave functions of the condensate. In this respect it has a connection with electronic quantum holography [36], which, however, occurs at a macroscopic scale in superconducts.

To demonstrate holographic imaging of an external object, we place the JJ in a low-temperature MFM and measure its response to the local field induced by the MFM tip (for details, see the Supplementary [41]). The tip creates a monopole-like field with a large  $\simeq 190$  Oe field at the tip [43]. To reduce its invasiveness, we placed the tip at a significant height  $h \simeq 1.7 \mu\text{m}$  above the center of the JJ. The black line in Fig. 3 shows corresponding experimental  $I_c(H)$  modulation. Even at this height the tip strongly shifts and distorts the  $I_c(H)$  pattern. The black

line in Fig. 3 (h) shows reconstructed tip-induced phase shift  $\varphi^*(x)$ . The blue line is a smooth fit, the derivative of which yields the tip-induced field, shown by the blue line in Fig. 3 (i). The red line in (i) represents the expected tip field at the tip-JJ height of  $\simeq 1.7 \mu\text{m}$  [41]. The agreement is very good. To cross check the correctness, we also calculated expected  $I_c(H)$  modulation for the reconstructed  $\varphi^*$ . It is shown by the red line in Fig. 3 (g). The agreement with experimental  $I_c(H)$  is good, confirming the validity of reconstruction.

Finally, we discuss advantages of the planar geometry. Although the holographic method is applicable to any type of JJs, good resolution requires 5-10 lobes of  $I_c(H)$  and the field range  $\pm 5 - 10 H_0$ . This field should be small enough to be noninvasive for both object and sensor. Therefore, JJs with a high field sensitivity (small  $H_0$ ) are preferred. In this respect, planar JJs with inherently small  $H_0$  [29, 31] have a major advantage compared to conventional overlap JJs. For our JJs  $H = 6 - 8$  Oe, see Figs. 3 (a-c), is sufficient for achieving the spatial accuracy of  $\sim 20$  nm. Furthermore, as demonstrated in Ref. [29], the planar geometry allows simple implementation of a control line for producing homogeneous magnetic field locally in the JJ. This facilitates acquisition of many  $I_c(H)$  lobes without disturbance of the object.

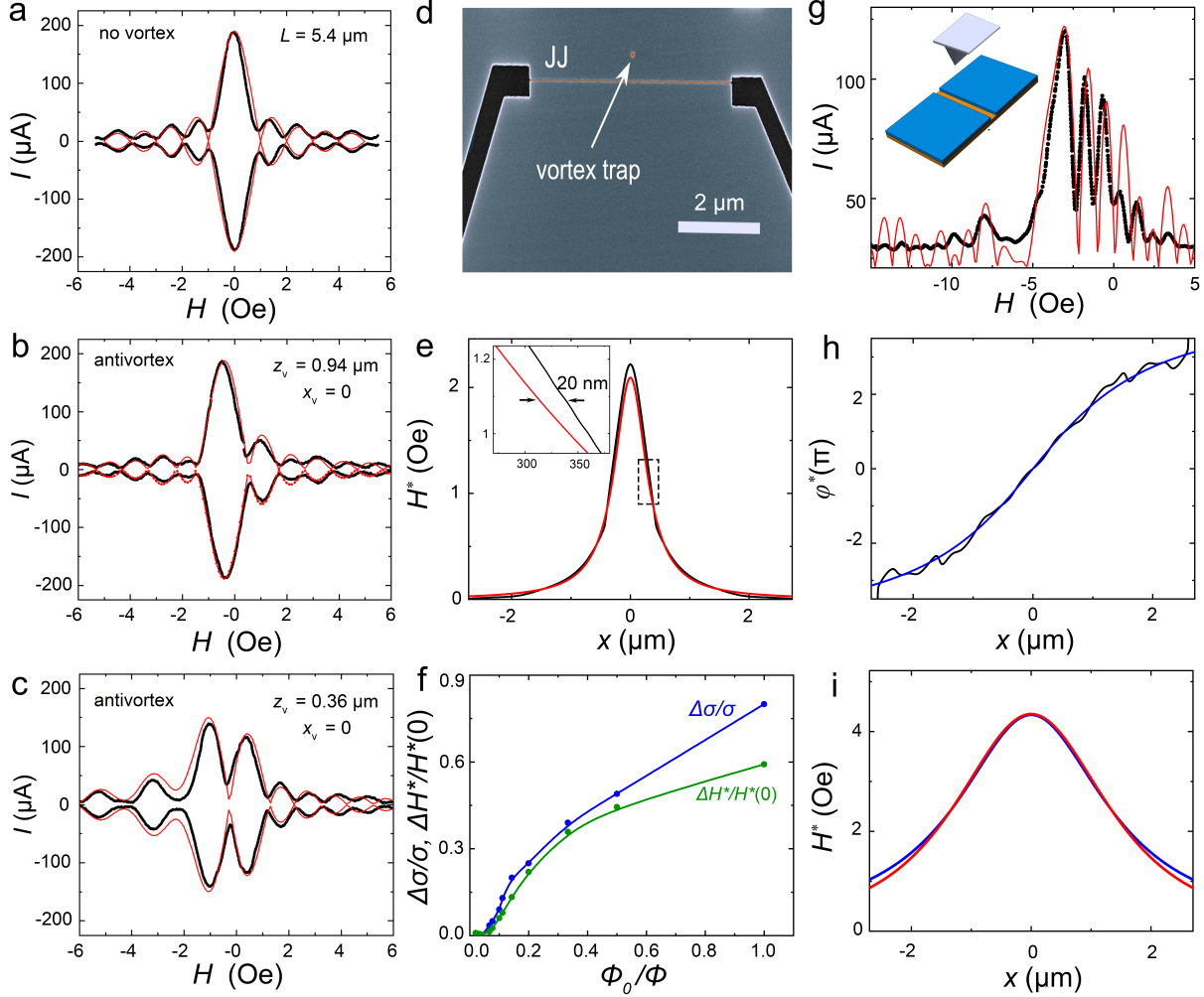


FIG. 3. Experimental verification of holographic reconstruction of a field from Abrikosov vortex in the junction electrode (a-c,e) and external MFM tip (g-i). (a-c) Measured  $I_c(H)$  (black symbols) (a) without a vortex and with a trapped antivortex at (b)  $z_v = 0.94 \mu\text{m}$  and (c)  $z_v = 0.36 \mu\text{m}$  from a junction. Red lines show fits, using Eq. (6). (d) SEM image of a planar Nb-CuNi-Nb junction with a vortex trap (false color). (e) Field profiles from AV. The back line represents holographic reconstruction of the experimental  $I_c(H)$  pattern from (c). The red line shows the expected profile from the corresponding fit by Eq. (6). The inset represents a close-up on the half-maximum region and demonstrates the spatial accuracy of reconstruction of  $\sim 20 \text{ nm}$ . (f) The relative accuracy of reconstruction versus the inverse flux range  $\Phi_0/\Phi$  for the case in (c). Blue and olive symbols show the relative accuracy of the width at half-maximum,  $\Delta\sigma/\sigma$ , and height of the maximum  $\Delta H^*/H^*(0)$ , respectively. (g) Black symbols represent measured  $I_c(H)$  pattern with MFM tip at  $h \simeq 1.7 \mu\text{m}$  above the JJ, as sketched in the inset. Red line represents  $I_c(H)$  calculated using the reconstructed  $\varphi^*(x)$ . (i) Reconstructed tip-induced phase shift in the JJ (black) and its spline (blue). (h) Field of the tip obtained from the reconstructed  $\varphi^*(x)$  (blue) and the anticipated monopole-like tip field at the tip height of  $\simeq 1.7 \mu\text{m}$  (red).

The ultimate field resolution of such sensor is determined by the flux noise. For our JJs it is  $\sim 10^{-7} \Phi_0 / \sqrt{Hz}$  at  $T = 4.2 \text{ K}$  [29]. Taking into account the flux quantization field  $H_0 \simeq 1 \text{ Oe}$ , it translates to the ultimate field sensitivity of  $10^{-11} \text{ Oe} / \sqrt{Hz}$ . It is remarkable that, contrary to conventional imaging techniques, which suffer from the trade-off problem between sensitivity and reso-

lution, in the discussed holographic method the high field sensitivity is *accompanied* by the high spatial resolution.

To conclude we derived theoretically and verified experimentally a novel method of magnetic image reconstruction by a single Josephson junction. The method resembles the holography, with the diffraction-like  $I_c(H)$  pattern serving as a hologram. It allows super-resolution

image reconstruction with nano-scale spatial resolution not limited by the junction size. The method allows obviating of the trade-off problem between sensitivity and resolution, typical for conventional imaging techniques, which directly probe the total flux or field in a sensor. We demonstrated that application of a planar Josephson junction for such holographic imaging facilitates both high field sensitivity and high spatial resolution, which is

beneficial for scanning probe microscopy.

## ACKNOWLEDGMENTS

We are gratefully to V.V. Dremov, S.Yu. Grebenchuk and V.S. Stolyarov for stimulating discussions and assistance with MFM measurements.

- 
- [1] H. J. Hug, B. Stiefel, P. Van Schendel, A. Moser, R. Hofer, S. Martin, H.-J. Guntherodt, S. Porthun, L. Abellmann, J. Lodder, G. Bochi and R. C. O’Handley, Quantitative magnetic force microscopy on perpendicularly magnetized samples, *J. Appl. Phys.* **83**, 5609 (1998).
  - [2] A. Volodin, K. Temst, C. Van Haesendonck, Y. Bruynseraede, M. Montero, and I. K. Schuller, Magnetic-force microscopy of vortices in thin niobium films: Correlation between the vortex distribution and the thickness dependent film morphology, *Europhys. Lett.* **58**, 582 (2002).
  - [3] H. Polshyn, T. R. Naibert, and R. Budakian, Imaging phase slip dynamics in micron-size superconducting rings, *Phys. Rev. B* **97**, 184501 (2018).
  - [4] T. R. Naibert, H. Polshyn, R. Garrido-Menacho, M. Durkin, B. Wolin, V. Chua, I. Mondragon-Shem, T. Hughes, N. Mason, and R. Budakian, Imaging and controlling vortex dynamics in mesoscopic superconductor–normal-metal–superconductor arrays, *Phys. Rev. B* **103**, 224526 (2021).
  - [5] H. Polshyn, T. Naibert, and R. Budakian, Manipulating multivortex states in superconducting structures, *Nano Lett.* **19**, 5476 (2019).
  - [6] V. V. Dremov, S. Y. Grebenchuk, A. G. Shishkin, D. S. Baranov, R. A. Hovhannisyan, O. V. Skryabina, N. Lebedev, I. A. Golovchanskiy, V. I. Chichkov, C. Brun, T. Cren, V. M. Krasnov, A. A. Golubov, D. Roditchev and V. S. Stolyarov, Local Josephson vortex generation and manipulation with a magnetic force microscope, *Nat. Commun.* **10**, 4009 (2019).
  - [7] S. Y. Grebenchuk, R. A. Hovhannisyan, V. V. Dremov, A. G. Shishkin, V. I. Chichkov, A. A. Golubov, D. Roditchev, V. M. Krasnov, and V. S. Stolyarov, Observation of interacting Josephson vortex chains by magnetic force microscopy, *Phys. Rev. Res.* **2**, 023105 (2020).
  - [8] J. R. Kirtley and J. P. Wikswo Jr, Scanning SQUID microscopy, *Ann. Rev. Mat. Sc.* **29**, 117 (1999).
  - [9] M. E. Huber, N. C. Koshnick, H. Bluhm, L. J. Archuleta, T. Azua, P. G. Bjornsson, B. W. Gardner, S. T. Halloran, E. A. Lucero, and K. A. Moler, Gradiometric micro-SQUID susceptometer for scanning measurements of mesoscopic samples, *Rev. Sc. Instr.* **79**, 053704 (2008).
  - [10] V. Bouchiat, Detection of magnetic moments using a nano-SQUID: limits of resolution and sensitivity in nearfield squid magnetometry, *Supercond. Sc. Technol.* **22**, 064002 (2009).
  - [11] C. Granata and A. Vettoliere, Nano superconducting quantum interference device: A powerful tool for nanoscale investigations, *Phys. Rep.* **614**, 1 (2016).
  - [12] J. R. Kirtley, L. Paulius, A. J. Rosenberg, J. C. Palmstrom, C. M. Holland, E. M. Spanton, D. Schiessl, C. L. Jermain, J. Gibbons, Y.-K.-K. Fung, M. E. Huber, D. C. Relp, M. B. Ketchen, G. W. Gibson, K. A. Moler, Scanning squid susceptometers with sub-micron spatial resolution, *Rev. Sc. Instr.* **87**, 093702 (2016).
  - [13] D. Vasyukov, Y. Anahory, L. Embon, D. Halbertal, J. Cuppens, L. Neeman, A. Finkler, Y. Segev, Y. Myasoedov, M. L. Rappaport, M. E. Huber and E. Zeldov, A scanning superconducting quantum interference device with single electron spin sensitivity, *Nat. Nanotechnol.* **8**, 639 (2013).
  - [14] A. Uri, A. Y. Meltzer, Y. Anahory, L. Embon, E. O. Lachman, D. Halbertal, N. Hr, Y. Myasoedov, M. E. Huber, A. F. Young and E. Zeldov, Electrically tunable multiterminal squid-on-tip, *Nano Lett.* **16**, 6910 (2016).
  - [15] P. Josephs-Franks, L. Hao, A. Tzalenchuk, J. Davies, O. Kazakova, J. Gallop, L. Brown, and J. Macfarlane, Measurement of the spatial sensitivity of miniature squids using magnetic-tipped STM, *Supercond. Sc. Technol.* **16**, 1570 (2003).
  - [16] L. Embon, Y. Anahory, Z. L. Jelic, E. O. Lachman, Y. Myasoedov, M. E. Huber, G. P. Mikitik, A. V. Silhanek, M. V. Milosevic, A. Gurevich, and E. Zeldov, Imaging of super-fast dynamics and flow instabilities of superconducting vortices, *Nat. Commun.* **8**, 85 (2017).
  - [17] A. Grigorenko, S. Bending, T. Tamegai, S. Ooi, and M. Henini, A one-dimensional chain state of vortex matter, *Nature* **414**, 728 (2001).
  - [18] B. Kalisky, J. Kirtley, E. Nowadnick, R. Dinner, E. Zeldov, Ariando, S. Wenderich, H. Hilgenkamp, D. Feldmann, and K. Moler, Dynamics of single vortices in grain boundaries: I-V characteristics on the femtovolt scale, *Appl. Phys. Lett.* **94**, 202504 (2009).
  - [19] P. Maletinsky<sup>1</sup>, S. Hong, M. S. Grinolds, B. Hausmann, M. D. Lukin, R. L. Walsworth, M. Loncar and A. Yacoby, A robust scanning diamond sensor for nanoscale imaging with single nitrogen-vacancy centres, *Nat. Nanotechnol.* **7**, 320 (2012).
  - [20] L. Rondin, J.-P. Tetienne, P. Spinicelli, C. Dal Savio, K. Karrai, G. Dantelle, A. Thiaville, S. Rohart, J.-F. Roch, and V. Jacques, Nanoscale magnetic field mapping with a single spin scanning probe magnetometer. *Appl. Phys. Lett.* **100**, 153118 (2012).
  - [21] Q.-C. Sun, T. Song, E. Anderson, A. Brunner, J. Förster, T. Shalomayeva, T. Taniguchi, K. Watanabe, J. Gräfe, Rainer Stöhr, X. Xu, and Jörg Wrachtrup, Magnetic domains and domain wall pinning in atomically thin CrBr<sub>3</sub> revealed by nanoscale imaging. *Nat. Commun.* **12**, 1989 (2021).
  - [22] J.P. Tetienne, A. Lombard, D. A. Simpson, C. Ritchie, J. Lu, P. Mulvaney, and L. C. L. Hollenberg, Scanning

- Nanospin Ensemble Microscope for Nanoscale Magnetic and Thermal Imaging, *Nano Lett.* **16**, 326 - 333 (2016).
- [23] M. Barbiero, S. Castelletto, Q. Zhang, Y. Chen, M. Charnley, S. Russelle, and M. Gu, Nanoscale magnetic imaging enabled by nitrogen vacancy centres in nanodiamonds labelled by iron-oxide nanoparticles, *Nanoscale* **12**, 8847–8857 (2020).
- [24] D. Koelle, R. Kleiner, F. Ludwig, E. Dantsker, and J. Clarke, High-transition-temperature superconducting quantum interference devices, *Rev. Mod. Phys.* **71**, 631 (1999).
- [25] F. Arute, K. Arya, R. Babbush, D. Bacon, J. C. Bardin, R. Barends, R. Biswas, S. Boixo, F. G. S. L. Brandao, D. A. Buell, B. Burkett, Yu Chen, Z. Chen, B. Chiaro, R. Collins, W. Courtney, A. Dunsworth, E. Farhi, B. Foxen, A. Fowler, C. Gidney, M. Giustina, R. Graff, K. Guerin, S. Habegger, M. P. Harrigan, M. J. Hartmann, Alan Ho, M. Hoffmann, T. Huang, T. S. Humble, S. V. Isakov, E. Jeffrey, Z. Jiang, D. Kafri, K. Kechedzhi, J. Kelly, P. V. Klimov, S. Knysh, A. Korotkov, F. Kostritsa, D. Landhuis, M. Lindmark, E. Lucero, D. Lyakh, S. Mandrà, J. R. McClean, M. McEwen, A. Megrant, X. Mi, K. Michielsen, M. Mohseni, J. Mutus, O. Naaman, M. Neeley, C. Neill, M. Y. Niu, E. Ostby, A. Petukhov, J. C. Platt, C. Quintana, E. G. Rieffel, P. Roushan, N. C. Rubin, D. Sank, K. J. Satzinger, V. Smelyanskiy, K. J. Sung, M. D. Trevithick, A. Vainsencher, B. Villalonga, T. White, Z. J. Yao, P. Yeh, A. Zalcman, H. Neven and J. M. Martinis, Quantum supremacy using a programmable superconducting processor, *Nature* **574**, 505 (2019).
- [26] A. Kandala, K. Temme, A. D. Corcoles, A. Mezzacapo, J. M. Chow, and J. M. Gambetta, Error mitigation extends the computational reach of a noisy quantum processor, *Nature* **567**, 491 (2019).
- [27] A. Barone and G. Paterno, Physics and applications of the Josephson effect (Wiley, 1982).
- [28] B. Plourde and D. Van Harlingen, Design of a scanning josephson junction microscope for submicron-resolution magnetic imaging, *Rev. Sc. Instr.* **70**, 4344 (1999).
- [29] T. Golod, O. Kapran, and V. Krasnov, Planar superconductor-ferromagnet-superconductor josephson junctions as scanning-probe sensors, *Phys. Rev. Appl.* **11**, 014062 (2019).
- [30] V. Kogan, V. Dobrovitski, J. Clem, Y. Mawatari, and R. Mints, Josephson junction in a thin film, *Phys. Rev. B* **63**, 144501 (2001).
- [31] A. A. Boris, A. Rydh, T. Golod, H. Motzkau, A. Klushin, and V. M. Krasnov, Evidence for nonlocal electrodynamics in planar josephson junctions, *Phys. Rev. Lett.* **111**, 117002 (2013).
- [32] V. M. Krasnov, Josephson junctions in a local inhomogeneous magnetic field, *Phys. Rev. B* **101**, 144507 (2020).
- [33] A. M. Bruckstein, R. J. Holt, and A. N. Netravali, Holographic image representations: the fourier transform method, in International Conference on Image Analysis and Processing (Springer, 1997) pp. 30–37.
- [34] T. Latychevskaia and H.-W. Fink, Practical algorithms for simulation and reconstruction of digital in-line holograms, *Appl Optics* **54**, 2424 (2015).
- [35] A. P. Vetal, D. Singh, R. K. Singh, and D. Mishra, Reconstruction of apertured fourier transform hologram using compressed sensing, *Optics and Lasers in Eng.* **111**, 227 (2018).
- [36] C. R. Moon, L. S. Mattos, B. K. Foster, G. Zeltzer, and H. C. Manoharan, Quantum holographic encoding in a two-dimensional electron gas, *Nat. Nanotech.* **4**, 167 (2009).
- [37] T. Golod, A. Pagliero, and V. M. Krasnov, Two mechanisms of josephson phase shift generation by an abrikosov vortex, *Phys. Rev. B* **100**, 174511 (2019).
- [38] T. Golod, R. A. Hovhannisyan, O. M. Kapran, V. V. Dremov, V. S. Stolyarov, and V. M. Krasnov, Reconfigurable josephson phase shifter, *Nano Lett.* **21**, 5240 (2021).
- [39] R. C. Dynes and T. A. Fulton, Supercurrent density distribution in josephson junctions, *Phys Rev. B* **3**, 3015 (1971).
- [40] V. Krasnov, V. Oboznov, and N. F. Pedersen, Fluxon dynamics in long josephson junctions in the presence of a temperature gradient or spatial nonuniformity, *Phys. Rev. B* **55**, 14486 (1997).
- [41] See the supplementary information at..., which contains additional description of: I. Experimental methods, II. Additional clarifications about inverse problem solution, III. Spatial resolution, IV. Image improvement methods
- [42] T. Golod, A. Rydh, and V. Krasnov, Detection of the phase shift from a single abrikosov vortex, *Phys. Rev. Lett.* **104**, 227003 (2010).
- [43] C. Di Giorgio, A. Scarfato, M. Longobardi, F. Bobba, M. Iavarone, V. Novosad, G. Karapetrov and A.M. Cucolo, Quantitative magnetic force microscopy using calibration on superconducting flux quanta, *Nanotechnology*, **30**, 314004 (2019).